ACS OMEGA

Open Access

http://pubs.acs.org/journal/acsodf

Article

Selective Manganese Precipitation via Neutralization and Ozone Oxidation under pH Conditions Similar to Steel Pickling Wastewater: Thermodynamic Assessment and Experimental XANES Evaluation

Mauricio Córdova-Udaeta, Bowen Cheng, Shigeshi Fuchida, Yutaro Takaya, Jun Horiuchi, Hiroyuki Masuoka, Keishi Oyama, and Chiharu Tokoro*

Cite This: *ACS Omega* 2025, 10, 18085−18097

Read Online

ACCESS | Metrics & More | Article Recommendations | Supporting Information

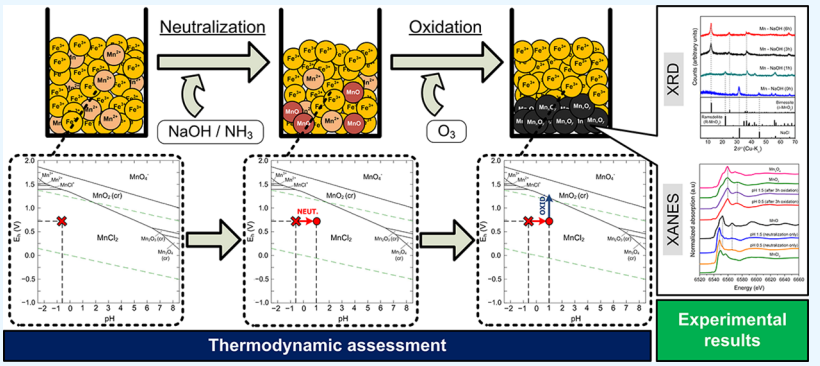

ABSTRACT: Steel pickling wastewater contains valuable iron. Nonetheless, coexisting elements such as Mn need to be separated before Fe recovery. This work studies Mn precipitation phenomena under a pH resembling steel pickling wastewater and compares it to that of Fe under the same conditions. A neutralization−oxidation approach was studied, whereby either NaOH or NH_3 were used as neutralizers and O_3 was the oxidizer. A thermodynamic assessment indicated that NaOH is more effective than NH_3 for precipitation because Mn can react freely with O_3 after NaOH addition, whereas NH_3 may react with O_3 instead. Experimental data showed that neutralization followed by oxidation results in the formation of different Mn oxides, with NaOH confirmed as the most effective neutralizer. Moreover, XRD and XANES analyses showed that the Mn oxidation state in the solids depends on the neutralizer used. Conversely, Fe precipitation was thermodynamically and experimentally observed to depend entirely on pH, with NaOH being a better neutralizer than NH_3, and pH = 1.5 being the maximum pH where Fe remains dissolved. These insights suggest that using a neutralization−oxidation method that increases the oxidation potential high enough for Mn oxidation while keeping the pH low enough for Fe to remain dissolved could be an effective approach for the selective precipitation of Mn from steel pickling wastewater.

1. INTRODUCTION

The steel industry is one of the largest industries worldwide, with production quantities surpassing 1800 Mt per year in 2020.[1,2] Due to the large volume and high demand, steel production generates large amounts of contaminants, such as dust, sludge, slag, and others.[3,4] Hence, steel manufacturers are looking for ways to minimize their environmental impact by improving the treatment methods of the waste streams released during their operations in order to increase their recyclability.[5]

The steel pickling process refers to a surface treatment directed at the removal of rust, scale, and unwanted oxides formed on the exterior layer of steel pieces, and is an industrial method that has a substantial environmental footprint.[3,6,7] Steel pickling is usually carried out by first cleaning the steel pieces mechanically and then cleaning their surface using the pickling process proper, where steel pieces are immersed in cleaning "baths" employing acids such as HNO_3, H_2SO_4, HCl, and HF, depending on the composition of the target product.[8,9]

This process generates large amounts of highly acidic wastewater, as the pickling bath can only be used a limited number of times before turning into a byproduct. Nonetheless, this wastewater usually contains several dissolved ions such as Fe^{2+}, Fe^{3+}, Cr^{3+}, Ni^{2+}, Zn^{2+}, Mn^{2+}, etc., which exceed the maximum limits set by regulations and thus constitute a heavy

Received: February 20, 2025
Revised: April 10, 2025
Accepted: April 17, 2025
Published: April 25, 2025

environmental burden.[10−13] Hence, performing a suitable treatment process for pickling wastewater would not only reduce the impact of the acid used but also be economically attractive for the steelmaking industry, as element recovery from wastewater could significantly reduce costs. In this regard, several studies have attempted to treat spent pickling liquors and separate the metallic elements (i.e., Zn, Cr, Mn, etc.) in order to obtain a concentrated acid solution containing only iron (Fe) ions. Afterward, this Fe-rich solution could be processed further to recover iron and recycled acid separately.[14] Thus, techniques like selective precipitation, membrane separation, diffusion dialysis, and solvent extraction, among others, can be found in the literature.[15−20]

However, there is a lack of research conducted on the treatment of acid pickling wastewater specifically containing manganese (Mn), even though significant amounts of Mn can be found in certain steel wastewaters.[21] In this case, the typical approaches for manganese removal using direct alkaline precipitation[22] or adsorption[23] may not be suitable due to the special characteristics of pickling wastewater. For instance, conventional alkaline precipitation will likely require a large amount of reagents for complete neutralization of highly acidic wastewater and will also have poor selectivity, as raising the pH inadequately would result in the formation of unwanted iron hydroxides. Similarly, the adsorption of Mn from pickling wastewater will be challenging not only because Mn^{2+} adsorption in the presence of large amounts of acid is rather limited[24] but also because any adsorbent material could be easily degraded at such low pH values.

On the other hand, the oxidation method for Mn^{2+} is a promising alternative, since it is well-known that Mn^{2+} can react with several oxidants under a wide range of pH conditions and precipitate various types of manganese oxides very efficiently.[25,26] This is because Mn^{2+} and Mn^{3+} oxides are very chemically active chemically, with the kinetically favored autocatalytic Mn^{2+} oxidation reaction readily taking place on their surface.[27−29] Then, if the medium conditions are controlled, the addition of an oxidant to an Mn^{2+} solution would initiate the in situ formation of highly active Mn oxides (i.e., MnO_2 and Mn_3O_4), which in turn will trigger the autocatalytic Mn^{2+} reaction and cause more Mn to oxidize. To achieve the conditions required for Mn^{2+} precipitation, ozone (O_3) can be utilized due to its high oxidation abilities. O_3 is also attractive because it has been utilized in different industrial wastewater applications to remove contaminants and for resource recovery.[30−33] However, using O_3 for the selective precipitation of manganese oxides under highly acidic conditions has been sparsely studied,[25] and the details of O_3 oxidation under conditions similar to steel pickling wastewater have not yet been thoroughly elucidated.

Therefore, the present research work focuses on studying a method involving neutralization followed by O_3 oxidation, in order to selectively precipitate Mn under conditions similar to those found in steel pickling wastewater (i.e., highly acidic). For this purpose, thermodynamic analyses and laboratory experiments were carried out for single systems where Mn and Fe are present independently, in order to gain an understanding of their respective behavior when subjected to the aforementioned neutralization−oxidation method. Subsequently, a mechanism for the phenomena occurring within each system is proposed. Lastly, the potential application for the selective precipitation of Mn from spent pickling wastewater is discussed based on the chemical insights obtained for each individual case.

2. MATERIALS AND METHODS

2.1. Thermodynamic Assessment of Systems Containing Individual Mn and Fe. A thermodynamic assessment was carried out for simulated systems resembling steel pickling wastewater using HCl as the acid (initial pH ≈ −0.6, $[Cl^-]$ concentration ≈4 M) containing either Mn or Fe individually. The Mn single system contained a Mn^{2+} concentration close to 1000 mg/L (approximately 0.018 M) as dissolved $MnCl_2$, whereas the Fe single system contained an Fe^{3+} concentration close to 75000 mg/L (approximately 1.34 M) as dissolved $FeCl_3$. Afterward, the addition of either NaOH or NH_3 was considered in these simulated systems in order to understand the effects of neutralization to a final pH of 0.5, 1.0, and 1.5, respectively. Additionally, oxidation with O_3 for each individual system was assumed to start from a conventional value (Eh ≈ 0.75 V) and reach the maximum water oxidation potential allowed at equilibrium under each pH condition. The above-mentioned assessment was performed using the SPANA software for geochemical calculations,[34] and several Eh−pH diagrams were prepared in order to develop insights into the chemical speciation of Mn and Fe under simulated conditions. For the sake of clarity, the concentrations used in these calculations are summarized in Table 1.

Table 1. Concentration of Chemical Species Used for the Eh−pH Diagrams

Parameter	pH of solution			Details
	0.5	1.0	1.5	
Cl^- concentration (M)	4.0	4.0	4.0	Initial HCl content (15%)
Mn^{2+} concentration (M)	0.018	0.018	0.018	For Mn single system
Fe^{3+} concentration (M)	1.34	1.34	1.34	For Fe single system
Neutralizer concentration (M)	3.68	3.90	3.96	For both NaOH and NH_3

2.2. Experimental Neutralization−Oxidation of the Mn Single System and Fe Single System. *2.2.1. Mn Single System.* First, a solution containing approximately 1000 ppm of Mn^{2+} was prepared using $MnCl_2$, regulated to a highly acidic environment (pH ≈ −0.6) using HCl to simulate the raw conditions found in steel pickling wastewater (approximately HCl concentration ≈ 15 wt %). Afterward, 300 g of this solution was neutralized using either NaOH (48 wt %) or NH_3 (28 wt %). In the case of NaOH, the solution was added slowly (approximately 15 g/min) until a final pH of 0.5, 1, and 1.5 was attained. Similarly, in the case of NH_3, the solution was added at around 15 g/min until the final pH achieved was 0.5 and 1.5. In both cases, after the desired pH had been obtained, the addition of an oxidizing agent (O_3 gas) to the system was started. For this purpose, a local ozone generator (ED-OG-RC12GC, EcoDesign Inc., Saitama, Japan) was used to bubble the O_3 gas at a dose equal to 1 L/min. Once the ozone bubbling had started, the oxidation took place, and samples were taken at different time intervals in order to analyze the elemental concentration in the liquid via ICP analysis (ICAP 6500 Duo, Thermo Fisher Scientific, Waltham, MA, USA). In addition, sample aliquots taken over time using either NaOH or NH_3 were retrieved, filtered using a 0.45 μm filter, washed

https://doi.org/10.1021/acsomega.5c01588
ACS Omega 2025, 10, 18085−18097

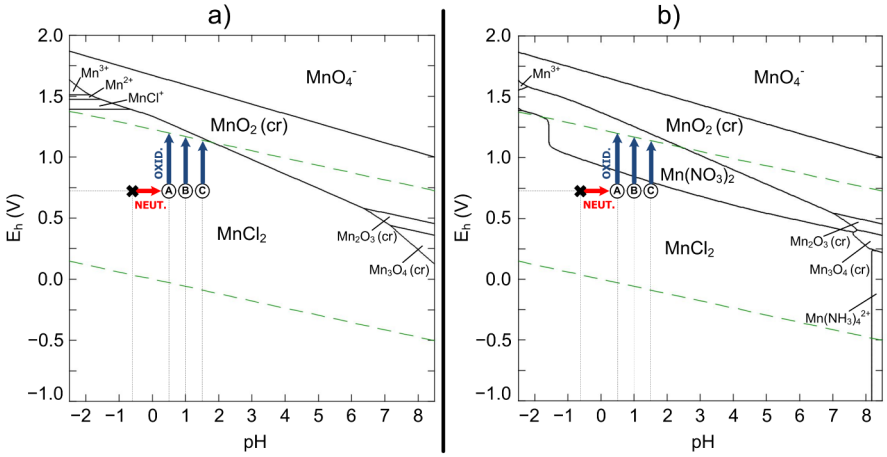

Figure 1. Eh−pH diagram for the simulated Mn single system. The boldface X in the diagram represents the starting point under highly acidic conditions (pH ≈ −0.6), and symbols (A), (B) and (C) represent the conditions after neutralization to pH values of 0.5, 1.0, and 1.5, respectively. The vertical arrows indicate the increase in oxidation potential due to O_3 addition. (a) Using NaOH as a neutralizer, (b) using NH_3 as a neutralizer.

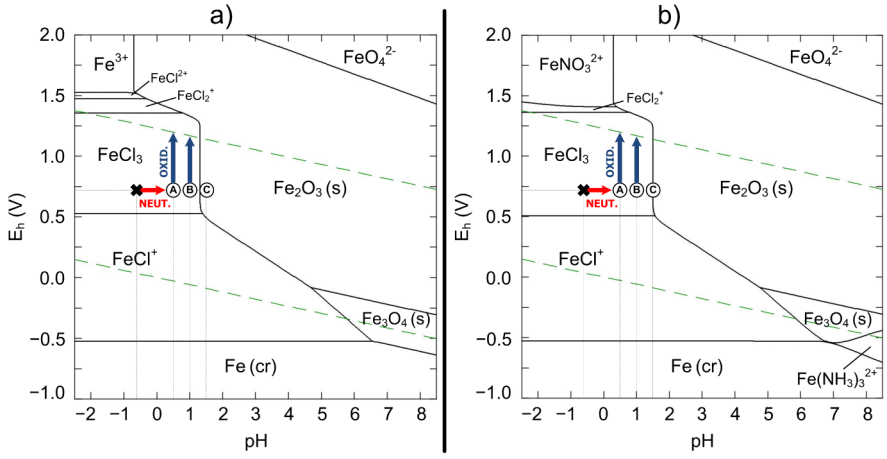

Figure 2. Eh−pH diagram for the simulated Fe single system. The boldface X in the diagram represents the starting point under initial highly acidic conditions (pH ≈ −0.6), and symbols (A), (B) and (C) represent the conditions after neutralization to pH values of 0.5, 1.0, and 1.5, respectively. The vertical arrows indicate the increase in oxidation potential due to O_3 addition. (a) Using NaOH as a neutralizer, (b) Using NH_3 as a neutralizer.

with water, and analyzed using XRD (SmartLab, SmartLab Studio, Database: ICDD PDF-2 Release 2020 RDB, Rigaku, Tokyo, Japan) and SEM-EDS (TM4000Plus, Hitachi High-Tech, Japan). Lastly, a selected group of solid samples and liquid samples were retrieved after neutralization and neutralization-oxidation at different times in order to identify their chemical speciation using XAFS analysis at the Mn K-Edge (BL11S2 beamline, Aichi Synchrotron Radiation Center, Aichi, Japan). For clarity, a schematic representation of the methodology described above is presented in Supplementary Figure 1.

2.2.2. Fe Single System. A mother liquor was prepared by dissolving 986 mL of concentrated HCl and using 968 g of $FeCl_3 \bullet 6H_2O$ to obtain a final solution of approximately 100000 ppm of Fe^{3+}. Afterward, samples of 300 g of this solution were neutralized using NaOH (48 wt %) and NH_3 (28 wt %), respectively. In this case, the final pH values obtained for both NaOH and NH_3 were 0.5, 1.0, and 1.5. Once the desired pH was attained, the same ozone generator described in section 2.2.1 was used to bubble the system with O_3 at 1 L/min. Once the bubbling began, samples were taken from the system at definite intervals and analyzed using ICP. In a similar fashion to the Mn single system, solids from the aliquots generated at prescribed times were collected, filtered, washed with water, and then analyzed using XRD and SEM-EDS. Furthermore, because it is well known that iron hydroxides are quickly formed after adding a neutralizer, XAFS analysis at the Fe K-edge was carried out only for the liquid phase after NaOH addition, in order to mainly focus on Fe speciation in solution. All the chemicals used in the experiments were of reagent grade and provided by Wako Pure Chemical, Osaka, Japan.

3. RESULTS AND DISCUSSION

3.1. Thermodynamic Assessment of Aqueous Systems. *3.1.1. Mn Single System.* The Eh−pH diagrams prepared for the neutralization of the single Mn system to a final pH of 1.5 are presented in Figure 1. It can be seen in Figure 1a that the NaOH neutralization process, shown as the horizontal red line spanning from pH ≈ −0.6 to either pH 0.5, 1.0, or 1.5, is predicted to not produce Mn precipitates on its own, as the speciation will favor the formation of soluble $MnCl_2$ until pH values closer to 5, when the oxidation potential is kept at Eh ≈ 0.75 V. However, the diagram

https://doi.org/10.1021/acsomega.5c01588
ACS Omega 2025, 10, 18085−18097

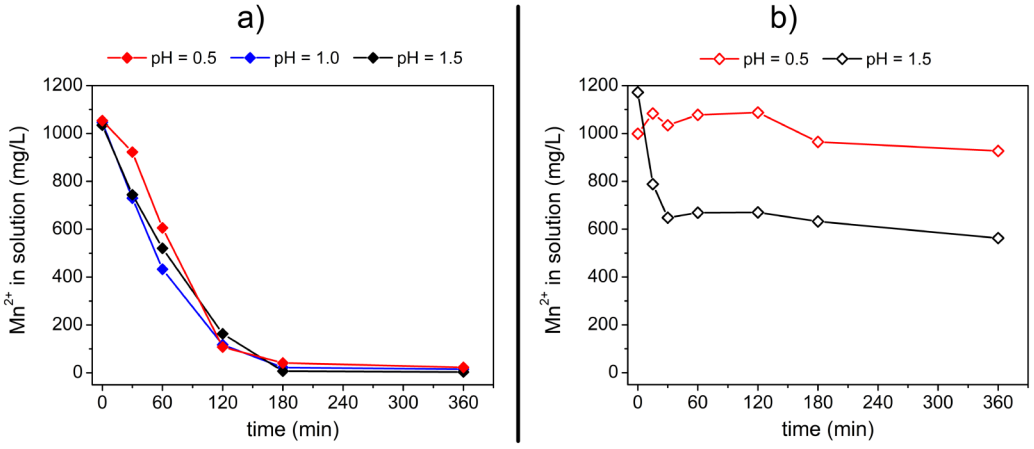

Figure 3. Mn^{2+} precipitation using neutralization followed by O_3 oxidation. (a) Using NaOH as a neutralizer, (b) using NH_3 as a neutralizer.

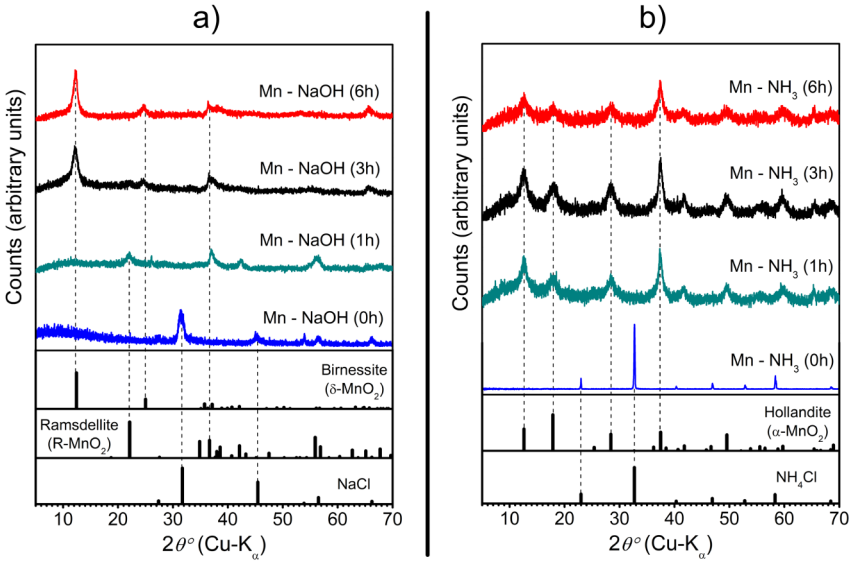

Figure 4. XRD results for Mn^{2+} precipitation using neutralization to a final pH = 1.5, followed by O_3 oxidation at different times. (a) Using NaOH as a neutralizer, (b) using NH_3 as a neutralizer.

predicts that the addition of O_3 (shown as the vertical blue arrows) will likely produce Mn oxides at pH 0.5, 1.0, or 1.5, since O_3 could easily increase the Eh oxidation potential in the system to values close to the equilibrium line where Mn solids (shown generically in the diagram as MnO_2) are expected.

Conversely, the case for NH_3 as a neutralizer is markedly different, as shown in Figure 1b. This is because the ammonium ion $(NH_4)^+$ in the system is predicted to react toward $(NO_3)^-$ under oxidizing conditions at high Eh values, which has been experimentally reported to occur in systems where transition metals and ozone are present.[35] Thus, the diagram clearly indicates that an intermediate region between $MnCl_2$ and MnO_2 will appear, whereby the nitrate $(NO_3)^-$ ion is combined with Mn^{2+} forming soluble $Mn(NO_3)_2$. This observation suggests that the direct reaction of O_3 with $(NH_4)^+$ will likely interfere with Mn^{2+} oxidation, resulting in less O_3 directly available for Mn precipitation.

3.1.2. Fe Single System. Figure 2 shows the Eh−pH diagrams for the Fe single system when a final pH of 1.5 is considered. It can be observed in Figure 2 that using either NaOH or NH_3 as a neutralizer will result in Eh−pH diagrams that are rather similar. It can also be seen in both Figure 2a,b that there is a clear vertical cutoff line in the region located between pH 1 and 2 for Eh values higher than 0.5 V. The existence of this line highlights the notorious effect of pH in terms of iron precipitation, as it indicates that soluble $FeCl_3$ abruptly changes to an insoluble form (shown in the diagrams generically as Fe_2O_3) once the pH is high enough. For instance, Figure 2a indicates that iron is expected to precipitate completely starting from pH values between 1.0 and 1.5 when NaOH is used as a neutralizer. Likewise, Figure 2b shows that iron is expected to precipitate at pH values higher than 1.5 for NH_3 addition. Furthermore, because the equilibrium regions where soluble $FeCl_3$ and insoluble Fe_2O_3 are separated by a vertical line completely parallel to the axis representing the oxidation potential (Eh), it can be inferred that the oxidation potential will practically not exert any significant influence on precipitation, regardless of the neutralizer employed.

3.2. Experimental Evaluation of Neutralization−Oxidation for Each Individual System. *3.2.1. Precipitation Experiments for the Mn Single System.* The results of the neutralization−oxidation experiments for the Mn single system are presented in Figure 3. In the case of Figure 3a, it can be seen that adding NaOH for neutralization before bubbling O_3

https://doi.org/10.1021/acsomega.5c01588
ACS Omega 2025, 10, 18085−18097

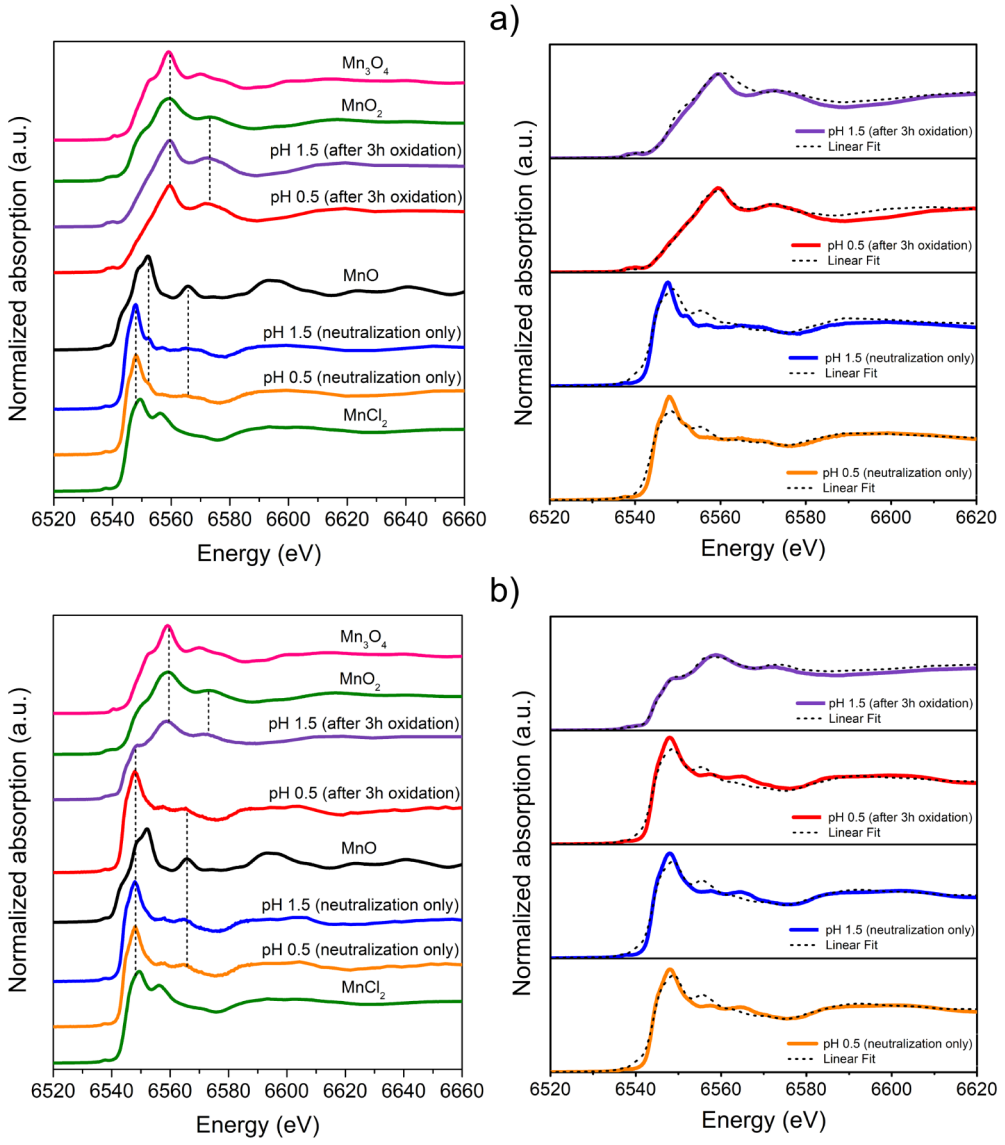

Figure 5. XAFS results for solid Mn samples obtained for neutralization followed by O_3 oxidation. XANES spectra is shown on the left side while the linear fitting results are shown on the right side. (a) Using NaOH as a neutralizer, (b) Using NH_3 as a neutralizer.

causes the concentration of Mn^{2+} to decrease noticeably, regardless of the final pH attained. It can also be observed that almost 100% of the initial Mn is removed from the solution after 180 min of reaction. Moreover, an inverse sigmoid trend can be seen for Mn^{2+} concentration curves, heavily implying that other phenomena besides direct Mn oxidation are taking place. In this regard, previous literature indicates that such behavior is typical of the kinetically favored autocatalytic Mn^{2+} precipitation,[27,29,36−38] which suggests the effectiveness of using NaOH before bubbling O_3 in terms of Mn precipitation.

Conversely, the concentration curves presented in Figure 3b indicate that the addition of NH_3 to the system before O_3 oxidation does not result in the complete precipitation of Mn^{2+} ions, regardless of the pH employed. In this case, it appears that the formation of Mn oxides is being limited, as no significant reduction in the Mn^{2+} concentration is observed even after 360 min of O_3 bubbling. This observation is in agreement with the diagram results presented in section 3.1.1, as it is likely that Mn oxidation is hindered when NH_3 is used for neutralization due to the formation of unwanted $(NO_3)^-$, and will always result in a significant amount of Mn^{2+} remaining in solution. Moreover, an inverse sigmoidal curve is not detected for the Mn concentration, suggesting that precipitation via Mn^{2+} autocatalysis is weakened.

3.2.2. Characterization of Precipitated Products from the Mn Single System. To characterize the products obtained experimentally, several XRD, SEM-EDS, and XAFS analyses were carried out for samples oxidized after NaOH and NH_3 addition. In the case of XRD analysis, the results shown in Figure 4a indicate that only a negligible amount of Mn oxides is formed immediately after NaOH addition at t = 0 h, with residual NaCl (PDF card: 01-080-3939) coming from HCl neutralization with NaOH being practically the only crystalline phase detected. After O_3 is added to the system, manganese oxides are detected at t = 1 h, with Ramsdellite (R-MnO_2, PDF card: 00-044-0142) observed as the main phase. Finally, the phase corresponding to Birnessite (δ-MnO_2, PDF card: 00-043-1456) is detected after oxidizing the system with O_3 for 3 h and onward. These results suggest that adding only NaOH will not result in significant Mn precipitation. Instead, it seems

https://doi.org/10.1021/acsomega.5c01588
ACS Omega 2025, 10, 18085−18097

Table 2. XANES Linear Fitting Results for the Mn Single System

Neutralizer	pH after neutralization	Oxidation time (h)	Fraction	$MnCl_2$ (%)	$Mn(NO_3)_2$ (%)	MnO (%)	Mn_3O_4 (%)	MnO_2 (%)	$(MnO_4)^-$ (%)
NaOH	0.5	0	Solid	75.5	-	24.5	-	-	-
	1.5	0	Solid	71.6	-	28.4	-	-	-
	0.5	3	Solid	-	-	35.3	12.2	52.4	-
	1.5	3	Solid	-	-	1.1	6.1	92.8	-
	0.5	0	Liquid	71.4	28.6	-	-	-	-
NH_3	0.5	0	Solid	79.5	-	20.5	-	-	-
	1.5	0	Solid	78.0	-	22.0	-	-	-
	0.5	3	Solid	79.4	-	19.3	-	1.3	-
	1.5	3	Solid	29.4	-	7.7	15.0	47.9	-
	0.5	0	Liquid	37.7	62.3	-	-	-	-
	0.5	3	Liquid	37.0	63.0	-	-	-	-
	1.5	3	Liquid	11.5	15.0	-	-	54.3	12.1

that O_3 bubbling is necessary to obtain Mn^{2+} oxides. Also, XRD results indicate that there is a change in the Mn oxide polymorph obtained, depending on the total oxidation time. This phenomenon could be attributed to stabilization changes from the tunneled structure of Ramsdellite toward the layered structure of sodium Birnessite, as Ramsdellite does not easily accommodate alkali cations such as Na^+ but rather accommodates (and becomes stabilized by) H^+ ions.[39]

In the case of NH_3 addition, Figure 4b shows that no Mn oxides are formed at t = 0 h, and that only the remainder of HCl neutralization, NH_4Cl (PDF card: 00-007-0007), is the only phase present. However, after bubbling O_3 for 1 h, the peaks corresponding to $(NH_4)^+$-intercalated Hollandite (α-MnO_2, PDF card: 01-082-1450) are detected. Because Hollandite is a stable manganese oxide with a tunneled structure known to hold positive ions such as K^+, Rb^{2+}, Cs^{2+}, Ba^{2+}, and $(NH_4)^+$ in its structure,[40] it is unlikely that further changes in the Mn polymorph will occur, as practically the same XRD pattern is observed for longer oxidation times (3 h and 6 h).

SEM-EDS analyses (see Supplementary Figure 2a) pointed out that using NaOH will result in particles with small granules on the surface after 1 h of O_3 oxidation, turning into particles with a higher degree of compaction after 3 h. It can also be seen that after 1 h of O_3 oxidation, the amount of Na within the particle is lower compared to 3 h of O_3 oxidation, as the EDS mapping for Na changes from a very diffuse distribution at 1 h to a more defined distribution after 3 h. These observations agree with the XRD results shown in Figure 4a, which indicate that as the O_3 bubbling time increases from 1 h to 3 h and beyond, the MnO_2 phase will shift from the proton-stabilized Ramsdellite (R-MnO_2) to Na-substituted Birnessite (δ-MnO_2). In contrast, SEM-EDS results for NH_3 introduced in Supplementary Figure 2b indicate that after 1 h of O_3 bubbling, the particles do not present visible granulation in the surface, while after 3 h of O_3 bubbling, the particles seem to have consolidated and formed a clear clump. Of particular note is the similar N content in the particles detected by SEM-EDS at 1 and 3 h. This suggests that once the oxidation process has started, the tunneled phase of ammonium Hollandite (α-MnO_2) forms, as suitable NH_4^+ migrates to its interior. Then, after reaching the maximum amount of NH_4^+ that can be intercalated, increasing the rate of O_3 oxidation beyond 1 h will not have a significant effect, in agreement with the XRD results shown in Figure 4b.

On the other hand, the XANES spectra results and the corresponding linear curve fitting for Mn oxides, shown in the lower sections of Figure 5a,b indicated that samples measured after the addition of neutralizer only (either NaOH or NH_3), would result in the formation of soluble $MnCl_2$ in the solids and a small amount of a Mn oxide represented by MnO. However, since MnO is thought to primarily contain the Mn cation as Mn^{2+}, it is likely that any solid oxide particle will go back to its dissolved form over time, as MnO is known to be rather soluble under acidic conditions.[41] This observation reinforces the hypothesis that simple neutralizer addition is poorly effective in achieving effective Mn precipitation.

However, for the XANES spectra and linear curve fitting shown in the upper section of Figure 5a, corresponding to NaOH neutralization followed by O_3 oxidation, it can be seen that the curves changed from resembling $MnCl_2$ to clearly matching the characteristic peaks of solid Mn species such as MnO_2 and Mn_3O_4. Furthermore, although both samples have XANES spectra that mostly resembles Birnessite,[42,43] the linear fitting indicated that the average Mn oxidation state found in the sample obtained at pH = 1.5 is markedly different when compared to the sample at pH = 0.5. In particular, the numerical results of linear curve fitting presented in Table 2 clearly show that neutralizing with NaOH to a higher pH before the addition of O_3 will lead to the formation of manganese solids with a higher oxidation state. Here, it can be seen that the oxides obtained at pH = 1.5 have a much higher content of Mn^{4+} (shown as MnO_2 %) when compared to the oxides obtained at pH = 0.5, which have a significant Mn content with lower oxidation states, such as Mn^{2+} (shown as MnO %) and $Mn^{2.67+}$ (shown as Mn_3O_4 %). Based on these observations, it can be inferred that a relationship exists between the initial pH reached before ozonation and the final oxidation state of Mn in the solids, with a higher initial pH value being directly correlated to a higher oxidation state.

Contrarily, in the case of NH_3 neutralization, the XANES spectra and linear curve fitting presented in the upper side of Figure 5b indicate that the oxidation of manganese is much more limited. For instance, the pH conditions of the medium during O_3 bubbling seem to exert an important role, as it can be observed that only the sample obtained at pH 1.5 moderately matched the spectra from MnO_2 and Mn_3O_4 standards. In comparison, the sample obtained at pH 0.5 still looks similar to the samples obtained after NH_3 neutralization only, whereby mostly soluble $MnCl_2$ is detected. Besides, the linear curve fitting hinted that it is necessary to increase the pH to values close to at least pH 1.5 when NH_3 is used in order to obtain Mn oxides with high oxidation states, as the numerical results shown in Table 2 suggested the presence of Mn^{4+}

https://doi.org/10.1021/acsomega.5c01588
ACS Omega 2025, 10, 18085−18097

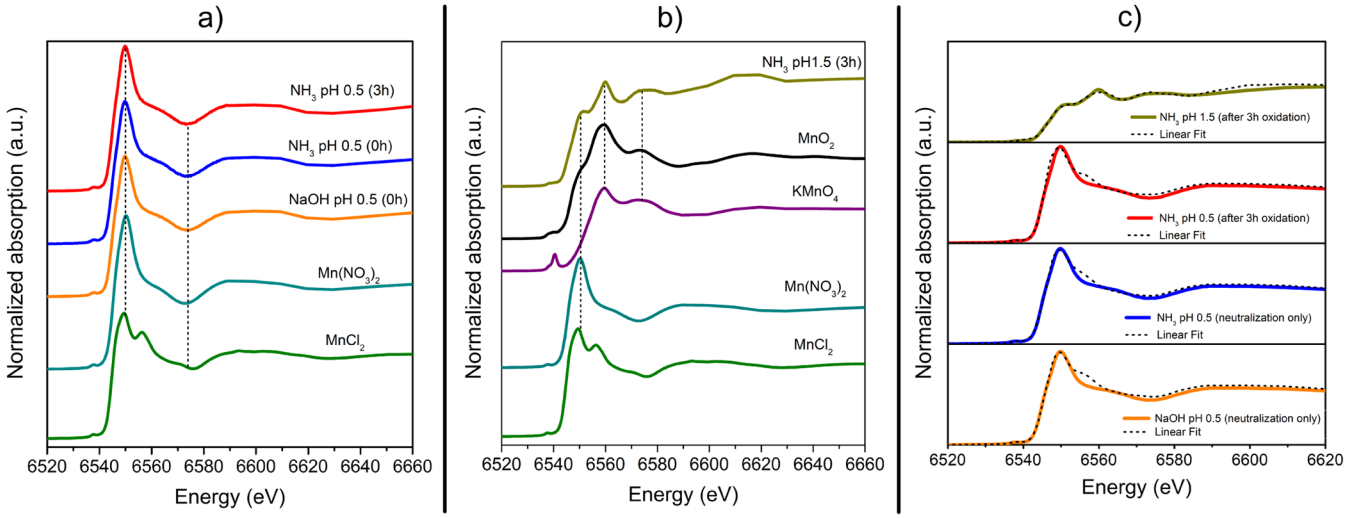

Figure 6. XAFS results for liquid Mn fractions obtained from the neutralization followed by O_3 oxidation at different times. (a) XANES spectra at a final pH = 0.5 for NaOH and NH_3, (b) XANES spectra at a final pH = 1.5 for NH_3 only, (c) linear fitting results for all samples.

(shown as MnO_2), $Mn^{2.67+}$ (shown as Mn_3O_4) and Mn^{2+} (shown as MnO).

In terms of the liquid, XANES results of the Mn single system are presented in Figure 6. In this case, the role of pH increase was also observed in terms of Mn speciation. For instance, at pH = 0.5, Figure 6a shows that both NaOH and NH_3 neutralization without O_3 bubbling result in only soluble species like $MnCl_2$ and $Mn(NO_3)_2$ in solution. Moreover, in the particular case of NH_3 neutralization, increasing the O_3 bubbling time to 3 h at pH 0.5 did not change the speciation at all, since Mn remained completely dissolved. However, when the pH for NH_3 neutralization was raised to pH = 1.5 before bubbling O_3 for 3 h, the XANES spectra changed, this time matching the pattern of oxidized Mn species as illustrated in Figure 6b. In particular, the results of linear fitting shown in Figure 6c and Table 2 indicated that, contrary to other samples for NH_3 neutralization, only the liquid at pH = 1.5 would have Mn oxidized toward Mn^{4+} (as MnO_2) and even Mn^{7+} (as $(MnO_4)^-$ instead of soluble Mn^{2+} as $MnCl_2$ or $Mn(NO_3)_2$. This means that unless the pH is high enough, Mn will not be easily oxidized in the presence of O_3 when NH_3 is the neutralizer. Rather, it appears that at low pH values, O_3 is likely to react with the ammonium ion $(NH_4)^+$ directly and produce $(NO_3)^-$ ions instead.

3.2.3. Discussion on the Precipitation Mechanism for the Mn Single System. Based on the thermodynamic analysis and the experimental results shown in the previous sections, it is clear that there is a fundamental difference between using NaOH or NH_3 during the neutralization step, not only in terms of Mn^{2+} precipitation efficiency but especially in terms of the crystalline phase of MnO_2 obtained. Therefore, the following explanation is proposed to elucidate the potential Mn reaction mechanisms involved for each neutralizer.

In the case of NaOH (a strong alkali), it is likely that an immediate reaction takes place each time an NaOH droplet is added, whereby $(OH)^-$ ions are released and react with Mn^{2+} ions nearby as follows:

$$Mn^{2+} + 2NaOH \rightarrow Mn(OH)_2 + 2Na^+ \quad (1)$$

Afterward, part of the $Mn(OH)_2$ formed may be redissolved back into Mn^{2+} due to the acidic conditions of the medium:

$$Mn(OH)_2 + 2H^+ \rightarrow Mn^{2+} + 2H_2O \quad (2)$$

However, if there are enough $(OH)^-$ ions in the immediate vicinity when NaOH is added, a fraction of the $Mn(OH)_2$ formed via reaction 1 can instead oxidize quickly and form MnOOH, as described below:[44,45]

$$Mn(OH)_2 + OH^- \rightarrow MnOOH + H_2O \quad (3)$$

Then, because it is known that MnOOH will go through disproportionation into MnO_2 and Mn^{2+} under acidic conditions, a further reaction could occur as follows:

$$2MnOOH + 2H^+ \rightarrow MnO_2 + Mn^{2+} + 2H_2O \quad (4)$$

Importantly, previous research has established that the MnO_2 phase formed via reaction 4 corresponds to Ramsdellite (R-MnO_2).[46] Furthermore, it is known that R-MnO_2 tends to be an intermediate phase that will eventually stabilize toward pyrolusite (β-MnO_2) or other more stable MnO_2 phases depending on the reaction conditions. Therefore, when the O_3 oxidation process starts, it is likely that the large amount of Na^+ existing in solution due to NaOH being used will exert a considerable influence on R-MnO_2 stabilization.[39] Because of this, the following transition from Ramsdellite to Na-intercalated Birnessite (δ-MnO_2) could take place:

$$R\text{-}MnO_2 \rightarrow \delta\text{-}MnO_2\ (Na^+\text{-intercalated}) \quad (5)$$

Importantly, δ-MnO_2 is known to be a very reactive manganese oxide due to its layered structure, which promotes the autocatalytic oxidation of Mn^{2+} under oxidizing conditions. Therefore, once the first Birnessite crystals are formed, the following simplified autocatalytic oxidation reaction for Mn^{2+} could take place during O_3 bubbling:

$$\delta\text{-}MnO_2 + Mn^{2+} + O_3 \rightarrow 2\delta\text{-}MnO_2 + 1/2O_2 \quad (6)$$

The series of steps proposed above could explain the autocatalytic curve presented in Figure 3a and the XRD results showing R-MnO_2 progressively transitioning toward Na-intercalated Birnessite. Moreover, this explanation aligns with the SEM-EDS results in Supplementary Figure 2a showing a lower amount of Na for an oxidation time equal to 1 h, and a larger amount of Na for an oxidation time equal to 3 h.

https://doi.org/10.1021/acsomega.5c01588
ACS Omega 2025, 10, 18085−18097

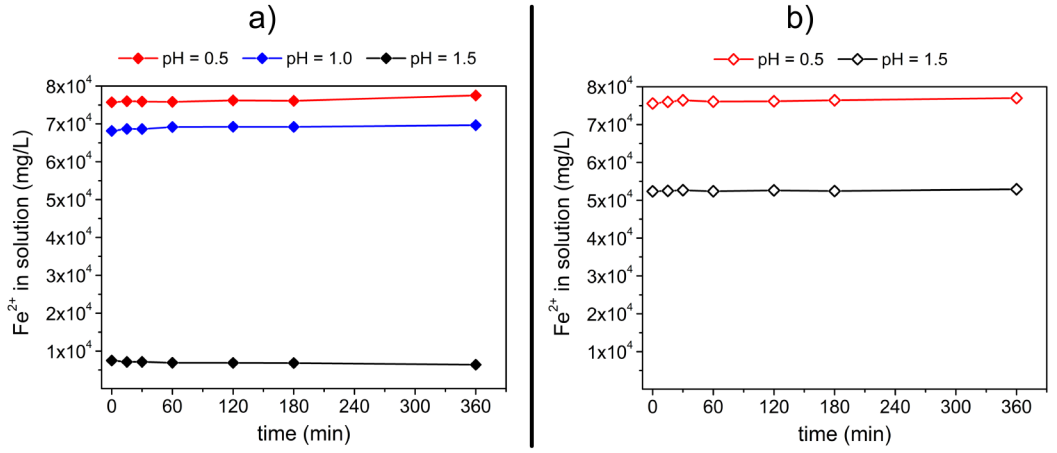

Figure 7. Fe^{3+} precipitation was carried out using neutralization followed by oxidation by O_3 oxidation. (a) Using NaOH as a neutralizer, (b) using NH_3 as a neutralizer.

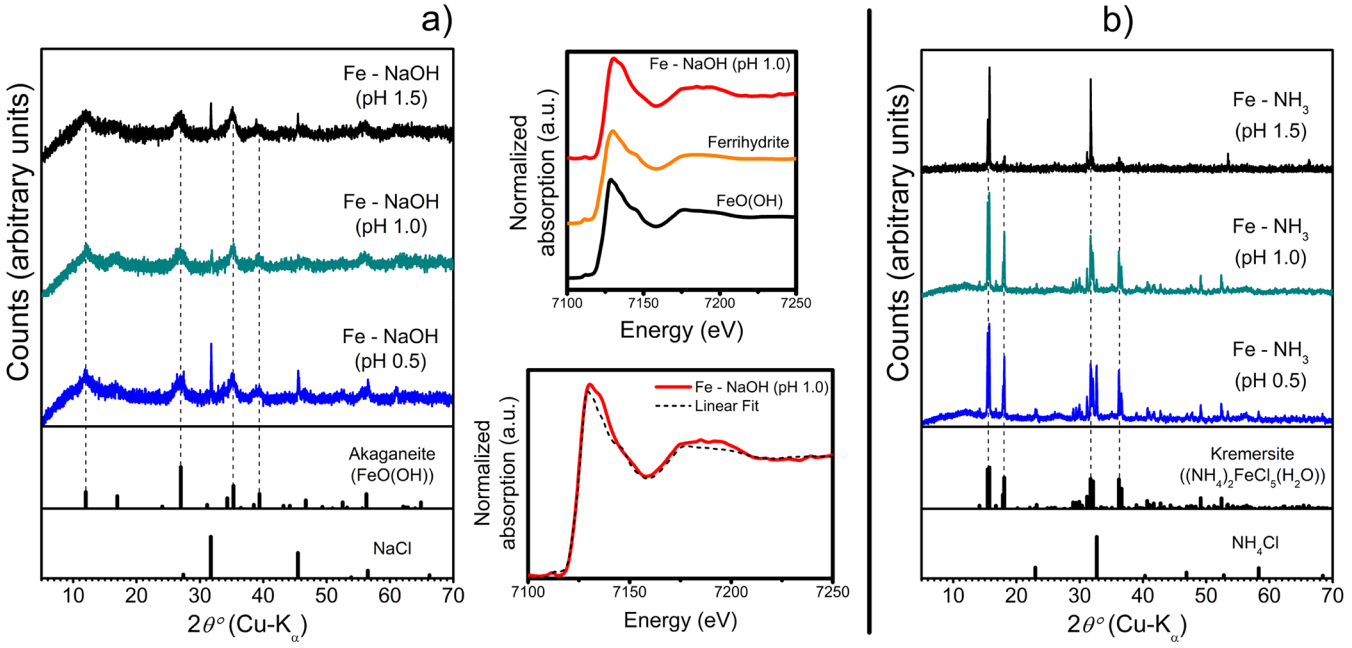

Figure 8. Characterization results for the solids obtained for the Fe single system were obtained using NaOH as a neutralizer. (a) XRD results for the Fe system using NaOH as a neutralizer (left side), and XANES spectra for a sample at pH = 1.0 with its linear fitting shown (right side). (b) XRD results for the Fe system using NH_3 as a neutralizer.

In the case of NH_3 neutralization, Mn^{2+} would react with aqueous NH_3 and result in $Mn(OH)_2$ as follows:

$$NH_3 + H_2O \leftrightharpoons NH_4^+ + OH^- \quad (7)$$

$$Mn^{2+} + 2NH_3 \rightarrow Mn(OH)_2 + 2NH_4^+ \quad (8)$$

However, because NH_3 is a much weaker alkali than NaOH (pK_b = 4.75), there are two main differences compared to the NaOH case. First, the amount of $Mn(OH)_2$ that could actually undergo reaction 3 will be reduced since the amount of $(OH)^-$ ions in the vicinity of each NH_3 droplet is lower, meaning that $Mn(OH)_2$ redissolution described in reaction 2 could outpace MnOOH formation. This fact may explain why there is no evident MnO_2 precipitation when NH_3 is added to a final pH = 0.5 (see Figure 3b). Thus, it is likely that any relevant amount of MnOOH will form only after adding enough NH_3 and reaching a high enough pH (i.e., pH = 1.5). Then, only the amount of MnOOH that was actually able to form will undergo disproportionation via reaction 4, resulting in R-MnO_2.

Second, because it is necessary to add large amounts of NH_3 to increase the pH to a sufficient level for $(OH)^-$ to promote reaction 3, an equally large amount of NH_4^+ will inevitably be added to the system. This would promote the following reaction, as NH_4^+ will interfere with O_3 oxidation:[35,47]

$$NH_4^+ + 4O_3 \rightarrow 2H^+ + (NO_3)^- + H_2O + 4O_2 \quad (9)$$

More importantly, because of the large amount of NH_4^+ ions in the system, the metastable phase of R-MnO_2 will not stabilize toward Birnessite as in the case with NaOH (reaction 5). Instead, the formation of $(NH_4)^+$-intercalated Hollandite-(α-MnO_2) would take place as follows:

$$\text{R-}MnO_2 \rightarrow \alpha\text{-}MnO_2\ (NH_4^+\text{-intercalated}) \quad (10)$$

https://doi.org/10.1021/acsomega.5c01588
ACS Omega 2025, 10, 18085−18097

Consequently, because Hollandite has a tunneled structure, the autocatalytic manganese reaction may be hampered when O_3 bubbling starts, and Mn^{2+} oxidation may happen through other, less efficient mechanisms. In summary, it is proposed that using NH_3 as a neutralizer results in a much lower amount of Mn oxides when compared to NaOH, not only because of NH_4^+ interference with O_3 as described in reaction 9, but also because of the lack of an efficient autocatalytic Mn reaction for $(NH_4)^+$-intercalated Hollandite, matching the experimental results presented in Figure 3b.

3.2.4. Precipitation Experiments for the Fe Single System. Our experiments indicated that Fe^{3+} precipitation behaves differently from Mn^{2+}, whereby the formation of solids occurs rather suddenly and in a single step. Hence, Figure 7a shows that the addition of NaOH to the Fe single system does not result in an appreciable formation of Fe oxides at pH 0.5, and only a small amount of precipitates forms at pH = 1.0. However, it was seen that precipitation proceeds readily at pH 1.5, resulting in the removal of virtually all Fe^{3+} and the formation of 100% solids immediately after the NaOH neutralization step. This indicates that O_3 oxidation is not relevant for the Fe single system and that only pH conditions control how much Fe remains in solution at any given time, which is in agreement with the vertical line existing between pH = 1 and pH = 2 in the Eh−pH diagram presented in Figure 2a.

Conversely, Figure 7b shows that the precipitation of Fe^{3+} is noticeably lower in the case of NH_3 addition, as solid formation is negligible at pH 0.5, while being only mildly effective at pH 1.5. Because Fe precipitation appears to be controlled by pH changes only, it is possible that a weak base such as NH_3 may not be alkaline enough to promote the formation of highly insoluble iron hydroxides unless added in large amounts and until pH values higher than 1.5 are obtained.

3.2.5. Characterization of Precipitated Products from the Fe Single System. The left side of Figure 8a shows the XRD results for Fe^{3+} precipitation after NaOH neutralization. Here, it can be observed that, regardless of the final pH, all the samples exhibited similar diffractograms, indicating the presence of residual NaCl from HCl neutralization and, more importantly, iron oxyhydroxides resembling Akaganeite (FeO(OH), PDF card: 00-034-1266), which is a phase commonly found during $FeCl_3$ neutralization.[48] The fact that FeO(OH)-like species are detected at all pH values suggests that the sole presence of $(OH)^-$ ions in the system is enough for the formation of insoluble Fe compounds. This is likely owing to their poor solubility and the large initial Fe^{3+} concentration, which would reach the saturation point rather easily.[49]

XANES results and linear curve fitting for the liquid fraction of the Fe system are shown on the right side of Figure 8a. It can be observed that the Fe sample at pH = 1.0 readily matches FeO(OH) and ferrihydrite standards. This was confirmed numerically, as the fitting indicated that approximately 92% of the spectra correspond to FeO(OH), and the rest (around 8%) correspond to ferrihydrite. These results could explain why using NaOH as a neutralizer causes more solids to form when compared to NH_3, since it is well-known that in the presence of sufficient $(OH)^-$ ions, Fe^{3+} undergoes deprotonation in solution followed by the formation of hydroxides of the type $(Fe(OH)_x)^{3-x}$, which are subsequently hydrolyzed toward FeO(OH) and ferrihydrite.[50−52] Moreover, since ferric oxyhydroxides are generally very insoluble,[49,53] the formation of FeO(OH) (akaganeite) would explain why having a higher pH after NaOH neutralization (for example, pH = 1.5) results in all Fe^{3+} being removed from the solution even before O_3 bubbling, in agreement with the Eh−pH diagram presented in Figure 2a.

In comparison, the XRD results shown in Figure 8b, corresponding to NH_3 as a neutralizer for the Fe single system, highlighted the formation of an iron-chloride complex in the presence of the $(NH_4)^+$ ion. In this case, the XRD peaks can be ascribed to Kremersite ($(NH_4)_2FeCl_5\bullet(H_2O)$), PDF card: 01-083-2193), which is the mineral analogue of diammonium aquopentachloroferrate.[54,55] This compound is a multiferroic material that has been reported to form when NH_4Cl and $FeCl_3$ react under various conditions, including the presence of HCl.[56,57] Hence, it is likely that the limited Fe^{3+} precipitation observed in Figure 7b when NH_3 is the neutralizer could be caused by the formation of the above-mentioned complex, which hinders the direct formation of insoluble iron oxyhydroxides even at pH = 1.5.

3.2.6. Discussion on the Precipitation Mechanism for the Fe Single System. Because both the thermodynamic simulation and experimental results indicated that Fe precipitation is controlled mainly by pH, the potential mechanism by which Fe precipitates in our system, presented below, will mostly disregard any effect of O_3 oxidation.

First, the following equilibrium describes $FeCl_3$ dissociation, which is common to both NaOH and NH_3 systems:

$$FeCl_3 \leftrightharpoons Fe^{3+} + 3Cl^- \quad (11)$$

Since it is known that Fe^{3+} can undergo hydrolysis and form several Fe oxyhydroxide species by reacting with water,[52,58] the following simplified reaction could describe the formation of FeO(OH):

$$Fe^{3+} + 2H_2O \leftrightharpoons FeO(OH) + 3H^+ \quad (12)$$

Now, because the initial conditions of our system are highly acidic (pH ≈ −0.6), the amount of H^+ is large, and the equilibrium is shifted to the left in reaction 12 at the beginning. However, when the strong base NaOH is used as a neutralizer, OH^- ions will react with H^+ as follows:

$$NaOH \rightarrow Na^+ + OH^- \quad (13)$$

$$OH^- + H^+ \rightarrow H_2O \quad (14)$$

Once reaction 14 occurs, the equilibrium presented in reaction 12 will inevitably shift to the right, promoting the quick precipitation of Fe oxyhydroxides due to immediate saturation.[49,59] At the same time, due to the large amounts of Na^+ and Cl^- present, NaCl would form concurrently as follows:

$$Na^+ + Cl^- \rightarrow NaCl \quad (15)$$

Experimental observations support the above-mentioned mechanism since a FeO(OH) phase (Akaganeite) was detected by XRD when NaOH was used as a neutralizer for pH 0.5, 1.0, and 1.5, with XAFS results clearly indicating the presence of FeO(OH) as well. In addition, SEM-EDS data shown in Supplementary Figure 3a highlighted the presence of Fe alongside O, indicating oxyhydroxides, whereas the presence of small NaCl incrustations in the particles supports the hypothesis of reactions 14 and (15)15 happening concurrently.

https://doi.org/10.1021/acsomega.5c01588
ACS Omega 2025, 10, 18085−18097

In the case of NH_3, it is likely that the direct formation of FeO(OH) via eq 12 will be hindered, since the amount of OH^- needed to promote neutralization is controlled by the weak base equilibrium presented in reaction 8. Therefore, in a similar fashion to that of the Mn^{2+} system, it will be necessary to provide a very large amount of NH_3 in order to meaningfully change the pH even a little, with a large amount of NH_4^+ being introduced to the system as a consequence. Because of this, and considering that a large amount of Cl^- was already present due to $FeCl_3$ dissociation and HCl content, the formation of the aquopentachloroferrate complex reaction would take place as follows:

$$Fe^{3+} + 5Cl^- + 2NH_4^+ + H_2O \rightarrow (NH_4)_2FeCl_5(H_2O) \quad (16)$$

Additionally, regardless of the final pH attained after neutralization, the large amount of NH_4^+ in the system would result in appreciable NH_4Cl formation as follows:

$$NH_4^+ + Cl^- \rightarrow NH_4Cl \quad (17)$$

The reaction steps introduced above correlate significantly with the experimental observations, since $(NH_4)_2FeCl_5(H_2O)$ was detected via XRD analysis, and SEM-EDS pictures shown in Figure 3b clearly highlight that Fe, Cl, and N coexist in the particles. Interestingly, SEM-EDS also showed that there is a small region where Fe and O are together, suggesting that a small amount of FeO(OH) will still precipitate via reaction 12 even in the case of NH_3 as a neutralizer, further supporting the postulated reaction series.

3.2.7. Discussion on the Potential Use of the Neutralization−Oxidation Method for Spent Pickling Wastewater Treatment. Even though the individual systems in this study were presented under simplified conditions, the results could be useful for discussing a neutralization−oxidation approach for the selective precipitation of Mn from spent pickling wastewater. For instance, Figure 9 shows the combined Eh−pH diagram for Mn and Fe systems based on the conditions presented in section 3.1, when NaOH is used as the neutralizer. It can be seen that there is an overlapping region at pH values between 0 and 1 and high oxidation potentials (above 1 V), where Fe is soluble (shown as $FeCl_3$) and Mn (shown as MnO_2) is insoluble. This region could become the target for a precipitation technique focused on the selective removal of Mn, since our results showed that Mn is much more dependent on oxidation potential for precipitation and that a mild neutralization with NaOH followed by O_3 bubbling would result in the complete oxidation of Mn^{2+}, even at comparatively "low" pH values like pH = 0.5 or pH = 1.0.

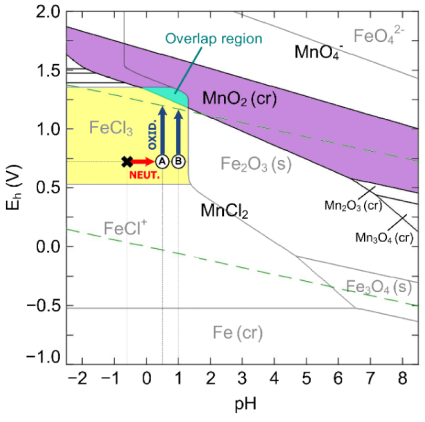

Figure 9. Combined Eh−pH diagram for Fe and Mn using the conditions described in Table 1 and NaOH as the neutralizer. The boldface X in the diagram represents the starting point under initial conditions (pH ≈ −0.6), and symbols (A) and (B) represent conditions after neutralization to a pH of 0.5 and 1.0, respectively. The vertical arrows indicate the increase in oxidation potential due to O_3 addition.

Likewise, because our experiments showed that Fe precipitation depends exclusively on pH, if the neutralization is carried out using NaOH in a controlled manner, then it might be possible to maintain Fe^{3+} in solution by keeping the pH below 1.0 before O_3 bubbling. Doing this would ensure that the formation of Fe-hydroxides like FeO(OH) is reduced to a minimum,[60] while keeping the conditions suitable for Mn oxidation.

Then, by combining these insights, the ideal neutralization−oxidation process for steel pickling wastewater containing Mn would use an NaOH neutralization step that never goes above pH 1.0, followed by an O_3 addition step carried out until the entirety of Mn^{2+} is precipitated, hence leaving the majority of Fe^{3+} ions in solution for further recovery. To illustrate this point, the flowchart presented in Figure 10 shows a potential technique for spent pickling wastewater based on the insights of this research work.

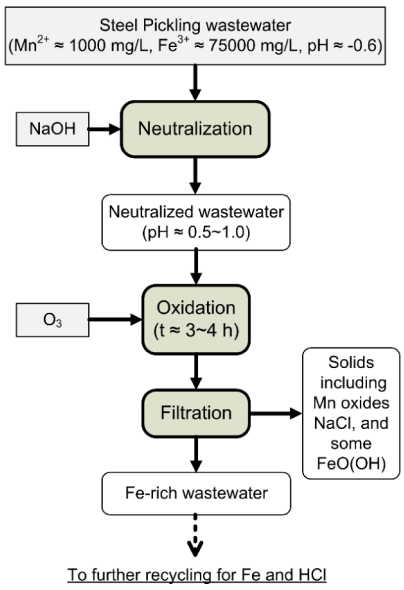

Figure 10. Flowchart for the potential application of a neutralization−oxidation process based on the results obtained in this research.

Nonetheless, in the case of real-world applications, it would also be necessary to consider potential surface reactions involved in the autocatalytic precipitation of Mn, alongside potential coprecipitation phenomena that may take place. For example, Mn oxides could capture amounts of partially hydrolyzed iron species, especially at the start of the precipitation, where nanocrystalline entities are expected before agglomeration into amorphous crystals.[57,61,62] Although this type of phenomenon could have an impact on the efficiency of the overall process, it is believed that the amount of FeO(OH) lost by coprecipitation would not be meaningful enough to offset the benefit of this technique, given the comparatively large amount of Fe^{3+} ions remaining in solution.

https://doi.org/10.1021/acsomega.5c01588
ACS Omega 2025, 10, 18085−18097

4. CONCLUSIONS

Results from this research pointed out that it is possible to precipitate Mn^{2+} under conditions similar to those of pickling wastewater using neutralization followed by O_3 oxidation. In particular, it was shown that NaOH is a neutralizer that is much more effective than NH_3. Additionally, it was seen that the Na-Birnessite (δ-MnO_2) phase found during NaOH neutralization is likely to induce the autocatalytic oxidation of Mn^{2+} as evidenced by the concentration curve behavior and XANES analysis, which showed the presence of typical autocatalytic products such as MnO_2 and Mn_3O_4 after O_3 bubbling.

In contrast, XANES results in the liquid and the thermodynamic analysis indicated the presence of the nitrate ion $(NO_3)^-$ for the case of NH_3 neutralization, hinting that an unwanted reaction of NH_4^+ interfering with O_3 is taking place. Moreover, XRD analysis suggested that the Mn^{2+} autocatalytic reaction may be inhibited as the comparatively less reactive phase of $(NH_4)^+$-Hollandite (α-MnO_2) was detected.

On the other hand, our results showed that Fe precipitation is controlled entirely by pH and that O_3 addition has no discernible effect on the system. Also, XANES analysis of the liquid indicated that Fe precipitation proceeds via the formation of Fe-hydroxides such as FeO(OH), suggesting that the strong base NaOH promotes more Fe precipitation than the weak base NH_3 owing to its greater capacity for iron hydroxylation.

Lastly, because our results showed that there is an overlapping Eh−pH region where Mn may form solid oxides, whereas Fe^{3+} may remain in solution, a potential method for the selective precipitation of Mn^{2+} from acid pickling wastewater was proposed. Hence, under ideal conditions, the proposed method would involve a neutralization step with NaOH until a pH between 0.5 and 1.0 is achieved, followed by O_3 oxidation until the majority of Mn^{2+} is precipitated. Finally, it is thought that the insights presented in this work contribute to a better understanding of Mn and Fe systems subjected to either neutralization or oxidation processes under highly acidic conditions.

■ ASSOCIATED CONTENT

Supporting Information

The Supporting Information is available free of charge at https://pubs.acs.org/doi/10.1021/acsomega.5c01588.

Schematic diagram for methodology used in the Mn^{2+} precipitation experiments (S1), SEM-EDS results for Mn solids (S2), SEM-EDS results for Fe solids (S3) (PDF)

■ AUTHOR INFORMATION

Corresponding Author

Chiharu Tokoro − *Department of Systems Innovation, Graduate School of Engineering, The University of Tokyo, Tokyo 113-8656, Japan; Faculty of Science and Engineering, Waseda University, Tokyo 169-8555, Japan;* orcid.org/0000-0001-6214-0402; Email: tokoro@waseda.jp

Authors

Mauricio Córdova-Udaeta − *Waseda Research Institute for Science and Engineering, Faculty of Science and Engineering, Waseda University, Tokyo 169-8555, Japan*

Bowen Cheng − *School of Creative Science and Engineering, Waseda University, Tokyo 169-8555, Japan*

Shigeshi Fuchida − *Department of Marine Resources and Environment, Tokyo University of Marine Science and Technology, Tokyo 108-8477, Japan*

Yutaro Takaya − *Department of Systems Innovation, Graduate School of Engineering, The University of Tokyo, Tokyo 113-8656, Japan*

Jun Horiuchi − *Functional Materials Research Department, JFE Steel Corporation, Chuo, Chiba 260-0835, Japan*

Hiroyuki Masuoka − *Functional Materials Research Department, JFE Steel Corporation, Chuo, Chiba 260-0835, Japan*

Keishi Oyama − *Department of Earth Resources Engineering, Graduate School of Engineering, Kyushu University, Fukuoka 819-0395, Japan*

Complete contact information is available at: https://pubs.acs.org/10.1021/acsomega.5c01588

Author Contributions

The manuscript was written by M.C.U. Experiments were performed under the supervision of J.H. and H.M. Sample characterization was carried out by C.B., K.O., and M.C.U. Additional revision and proofreading were performed by Y.T. and S.F. Supervision was provided by C.T. All authors have given their approval to the final version of the manuscript.

Notes

The authors declare no competing financial interest.

■ ACKNOWLEDGMENTS

This work was partially supported by the Ministry of Education, Culture, Sports, Science and Technology (MEXT), Japan. Part of this work was performed within the activities of the Research Institute for Science and Engineering, the Sustainable Energy & Environmental Society Open Innovation Research Organization (SEES), and the Kagami Memorial Research Institute for Materials Science and Technology, Waseda University. This work resulted from the use of research equipment (G1004, G1009, G1010, G1018) shared under the MEXT Project for Promoting Public Utilization of Advanced Research Infrastructure (Program for Supporting Construction of Core Facilities) (Grant Number JPMXS0440500023).

■ REFERENCES

(1) Hasanbeigi, A. *Steel Climate Impact- An International Benchmarking of Energy and CO2 Intensities*; Global Efficiency Intelligence: Florida, United States, 2022. https://www.globalefficiencyintel.com.

(2) Zhang, J.; Shen, H.; Chen, Y.; Meng, J.; Li, J.; He, J.; Guo, P.; Dai, R.; Zhang, Y.; Xu, R.; Wang, J.; Zheng, S.; Lei, T.; Shen, G.; Wang, C.; Ye, J.; Zhu, L.; Sun, H. Z.; Fu, T.-M.; Yang, X.; Guan, D.; Tao, S. Iron and Steel Industry Emissions: A Global Analysis of Trends and Drivers. *Environ. Sci. Technol.* **2023**, *57* (43), 16477−16488.

(3) Li, L.-F.; Celis, J.-P. PICKLING OF AUSTENITIC STAINLESS STEELS (A REVIEW). *Can. Metall. Q.* **2003**, *42* (3), 365−376.

(4) Nidheesh, P. V.; Kumar, M. S. An Overview of Environmental Sustainability in Cement and Steel Production. *J. Cleaner Prod.* **2019**, *231*, 856−871.

(5) Rawat, A.; Srivastava, A.; Bhatnagar, A.; Gupta, A. K. Technological Advancements for the Treatment of Steel Industry Wastewater: Effluent Management and Sustainable Treatment Strategies. *J. Cleaner Prod.* **2023**, *383*, 135382.

(6) Tang, B.; Su, W.; Wang, J.; Fu, F.; Yu, G.; Zhang, J. Minimizing the Creation of Spent Pickling Liquors in a Pickling Process with High-Concentration Hydrochloric Acid Solutions: Mechanism and Evaluation Method. *J. Environ. Manage* **2012**, *98*, 147−154.
(7) Yang, C.; Pan, J.; Zhu, D.; Guo, Z.; Li, X. Pyrometallurgical Recycling of Stainless Steel Pickling Sludge: A Review. *J. Iron Steel Res. Int.* **2019**, *26* (6), 547−557.
(8) Anderez, A.; Alguacil, F. J.; López, F. A. Acid Pickling of Carbon Steel. *Revmetal* **2022**, *58* (3), No. e226.
(9) Yang, F.; Wu, Y.; Fang, X.; Ma, L. Experimental and Theoretical Study on the Behaviour of a Pickling Solution: The Role of Ferrous Ions. *J. Cleaner Prod.* **2020**, *243*, 118631.
(10) Devi, A.; Singhal, A.; Gupta, R.; Panzade, P. A Study on Treatment Methods of Spent Pickling Liquor Generated by Pickling Process of Steel. *Clean Techn Environ. Policy* **2014**, *16* (8), 1515−1527.
(11) Liang, D.; Ji, M.; Zhu, S.; Chen, Y.; Wang, Z.; Liu, Y.; Khan, A.; Ri, K.; Yu, H.; Huo, M. A Novel Fe Recycling Method from Pickling Wastewater Producing a $KFeS_2$ Whisker for Electroplating Wastewater Treatment. *Environ. Sci.: water Res. Technol.* **2021**, *7* (8), 1480−1491.
(12) Rögener, F.; Sartor, M.; Bán, A.; Buchloh, D.; Reichardt, T. Metal Recovery from Spent Stainless Steel Pickling Solutions. *Resour., Conserv. Recycl.* **2012**, *60*, 72−77.
(13) Laso, J.; García, V.; Bringas, E.; Urtiaga, A. M.; Ortiz, I. Selective Recovery of Zinc over Iron from Spent Pickling Wastes by Different Membrane-Based Solvent Extraction Process Configurations. *Ind. Eng. Chem. Res.* **2015**, *54* (12), 3218−3224.
(14) Regel-Rosocka, M. A Review on Methods of Regeneration of Spent Pickling Solutions from Steel Processing. *J. Hazard. Mater.* **2010**, *177* (1−3), 57−69.
(15) Hermoso, J.; Dufour, J.; Gálvez, J. L.; Negro, C.; López-Mateos, F. Nickel Hydroxide Recovery from Stainless Steel Pickling Liquors by Selective Precipitation. *Ind. Eng. Chem. Res.* **2005**, *44* (15), 5750−5756.
(16) San Román, M. F.; Ortiz Gándara, I.; Ibañez, R.; Ortiz, I. Hybrid Membrane Process for the Recovery of Major Components (Zinc, Iron and HCl) from Spent Pickling Effluents. *J. Membr. Sci.* **2012**, *415−416*, 616−623.
(17) Samaniego, H.; San Román, M. F.; Ortiz, I. Kinetics of Zinc Recovery from Spent Pickling Effluents. *Ind. Eng. Chem. Res.* **2007**, *46* (3), 907−912.
(18) Negro, C.; Blanco, M. A.; López-Mateos, F.; DeJong, A. M. C. P.; LaCalle, G.; Van Erkel, J.; Schmal, D. Free acids and chemicals recovery from stainless steel pickling baths. *Sep. Sci. Technol.* **2001**, *36* (7), 1543−1556.
(19) Gao, Y.; Yue, T.; Sun, W.; He, D.; Lu, C.; Fu, X. Acid Recovering and Iron Recycling from Pickling Waste Acid by Extraction and Spray Pyrolysis Techniques. *J. Cleaner Prod.* **2021**, *312*, 127747.
(20) Marañón, E.; Fernández, Y.; Súarez, F. J.; Alonso, F. J.; Sastre, H. Treatment of Acid Pickling Baths by Means of Anionic Resins. *Ind. Eng. Chem. Res* **2000**, *39* (9), 3370−3376.
(21) Agrawal, A.; Sahu, K. K. An Overview of the Recovery of Acid from Spent Acidic Solutions from Steel and Electroplating Industries. *J. Hazard. Mater.* **2009**, *171* (1−3), 61−75.
(22) Nkele, K.; Mpenyana-Monyatsi, L.; Masindi, V. Challenges, advances and sustainabilities on the removal and recovery of manganese from wastewater: A review. *J. Cleaner Prod.* **2022**, *377*, 134152.
(23) Patil, D. S.; Chavan, S. M.; Oubagaranadin, J. U. K. A Review of Technologies for Manganese Removal from Wastewaters. *J. Environ. Chem. Eng.* **2016**, *4* (1), 468−487.
(24) Al-Wakeel, K. Z.; Abd El Monem, H.; Khalil, M. M. H. Removal of Divalent Manganese from Aqueous Solution Using Glycine Modified Chitosan Resin. *J. Environ. Chem. Eng.* **2015**, *3* (1), 179−186.
(25) Ching, S.; Suib, S. L. Synthetic Routes to Microporous Manganese Oxides. *Comments Inorg. Chem.* **1997**, *19* (5), 263−282.
(26) Chen, B.-R.; Sun, W.; Kitchaev, D. A.; Mangum, J. S.; Thampy, V.; Garten, L. M.; Ginley, D. S.; Gorman, B. P.; Stone, K. H.; Ceder, G.; Toney, M. F.; Schelhas, L. T. Understanding Crystallization Pathways Leading to Manganese Oxide Polymorph Formation. *Nat. Commun* **2018**, *9* (1), 2553.
(27) Allard, S.; Fouche, L.; Dick, J.; Heitz, A.; von Gunten, U. Oxidation of Manganese(II) during Chlorination: Role of Bromide. *Environ. Sci. Technol.* **2013**, *47* (15), 8716−8723.
(28) Morgan, J. J. Kinetics of Reaction between O2 and Mn(II) Species in Aqueous Solutions. *Geochim. Cosmochim. Acta* **2005**, *69* (1), 35−48.
(29) Córdova-Udaeta, M.; Cheng, B.; Fuchida, S.; Takaya, Y.; Oyama, K.; Tokoro, C. Insights on the Mechanism of Manganese Oxide Precipitation from Mn2+ Solutions Using NaClO Under Highly Acidic Conditions, via Experimental Observations and Numerical Fitting of the Kinetic ODE System. *J. Chem. Eng. Jpn* **2024**, *57* (1), 2366409.
(30) El Araby, R.; Hawash, S.; El Diwani, G. Treatment of Iron and Manganese in Simulated Groundwater via Ozone Technology. *Desalination* **2009**, *249* (3), 1345−1349.
(31) Shekarian, Y.; Hassas, B. V.; Rezaee, M.; Pisupati, S. V. Development of a Chemical-Free Process Utilizing Ozone Oxidative Precipitation for the Recovery of Cobalt and Manganese from Acid Mine Drainage. *J. Environ. Chem. Eng.* **2022**, *10* (5), 108533.
(32) Ghuge, S. P.; Saroha, A. K. Catalytic Ozonation for the Treatment of Synthetic and Industrial Effluents - Application of Mesoporous Materials: A Review. *J. Environ. Manage* **2018**, *211*, 83−102.
(33) Nishimura, T.; Umetsu, Y. Oxidative Precipitation of Arsenic(III) with Manganese(II) and Iron(II) in Dilute Acidic Solution by Ozone. *Hydrometallurgy* **2001**, *62* (2), 83−92.
(34) Puigdomènech, I.; Colàs, E.; Grivé, M.; Campos, I.; García, D. A Tool to Draw Chemical Equilibrium Diagrams Using SIT: Applications to Geochemical Systems and Radionuclide Solubility. *MRS Online Proc. Libr* **2014**, *1665* (1), 111−116.
(35) Ichikawa, S.; Mahardiani, L.; Kamiya, Y. Catalytic Oxidation of Ammonium Ion in Water with Ozone over Metal Oxide Catalysts. *Catal. Today* **2014**, *232*, 192−197.
(36) Coughlin, R. W.; Matsui, I. Catalytic Oxidation of Aqueous Mn(II). *J. Catal.* **1976**, *41* (1), 108−123.
(37) Lawrance, G. A.; Ward, C. B. Kinetics of Oxidation of Manganese(II) by Peroxomonosulfuric Acid in Aqueous Acidic Solution. *Transition Met. Chem.* **1985**, *10* (7), 258−261.
(38) Schuster, P. What Is Special about Autocatalysis? *Monatsh. Chem.* **2019**, *150* (5), 763−775.
(39) Kitchaev, D. A.; Dacek, S. T.; Sun, W.; Ceder, G. Thermodynamics of Phase Selection in MnO_2 Framework Structures through Alkali Intercalation and Hydration. *J. Am. Chem. Soc.* **2017**, *139* (7), 2672−2681.
(40) Feng, Q.; Horiuchi, T.; Mitsusio, T.; Yanagisawa, K.; Yamasaki, N. Hydrothermal Soft Chemical Synthesis of NH4+ Form of Hollandite-Type Manganese Oxide. *J. Mater. Sci. Lett.* **1999**, *18* (17), 1375−1378.
(41) Jones, C. F.; Smart, R. S.; Turner, C. P. S. Dissolution Kinetics of Manganese Oxides. Effects of Preparation Conditions, pH and Oxidation/Reduction from Solution. *Faraday Trans.* **1990**, *86* (6), 947.
(42) Hocking, R. K.; King, H. J.; Hesson, A.; Bonke, S. A.; Johannessen, B.; Fekete, M.; Spiccia, L.; Chang, S. L. Y. Engineering Disorder at a Nanoscale: A Combined TEM and XAS Investigation of Amorphous versus Nanocrystalline Sodium Birnessite. *Aust. J. Chem.* **2015**, *68* (11), 1715.
(43) Silvester, E.; Manceau, A.; Drits, V. A. Structure of Synthetic Monoclinic Na-Rich Birnessite and Hexagonal Birnessite; II, Results from Chemical Studies and EXAFS Spectroscopy. *Am. Mineral.* **1997**, *82* (9−10), 962−978.
(44) Hernandez Ubeda, M.; Mishima, H. T.; López De Mishima, B. A. The Electrochemical Response of Manganese Hydroxide—Oxide

https://doi.org/10.1021/acsomega.5c01588
ACS Omega 2025, 10, 18085−18097

Films in Slightly Alkaline Solutions—I. The Redox Couple. *Electrochim. Acta* **1991**, *36* (5−6), 1013−1018.
(45) Cha, D. K.; Park, S. Electrochemical Oxidation of Mn (OH) 2 in Alkaline Media. *J. Electrochem. Soc.* **1997**, *144* (8), 2573−2580.
(46) Ramstedt, M.; Sjöberg, S. Phase Transformations and Proton Promoted Dissolution of Hydrous Manganite (γ-MnOOH). *Aquat. Geochem.* **2005**, *11* (4), 413−431.
(47) Khuntia, S.; Majumder, S. K.; Ghosh, P. Removal of Ammonia from Water by Ozone Microbubbles. *Ind. Eng. Chem. Res.* **2013**, *52* (1), 318−326.
(48) Ryu, T.; Wada, S.-I. Preparation and characterization of thick and stable sol of β-feooh nano-particles. *Clay Science* **1999**, *10* (6), 497−502.
(49) Baumgartner, J. Iron Solubility, Colloids and Their Impact on Iron (Oxyhydr)Oxide Formation from Solution. *Earth-Sci. Rev.* **2015**, *150*, 520−530.
(50) Flynn, C. M. Hydrolysis of Inorganic Iron(III) Salts. *Chem. Rev.* **1984**, *84* (1), 31−41.
(51) Cornell, R. M.; Schwertmann, U. The Iron Oxides: Structure, Properties, Reactions, Occurrences and Uses, 2nd, Completely Revised and Extended Edition, *General Chemistry* 2nd ed. ed.; Wiley: Weinheim, 2003.
(52) Stefánsson, A. Iron(III) Hydrolysis and Solubility at 25 °C. *Environ. Sci. Technol.* **2007**, *41* (17), 6117−6123.
(53) Bailey, J. K.; Brinker, C. J.; Mecartney, M. L. Growth Mechanisms of Iron Oxide Particles of Differing Morphologies from the Forced Hydrolysis of Ferric Chloride Solutions. *J. Colloid Interface Sci.* **1993**, *157* (1), 1−13.
(54) Zolotarev, A. A.; Zhitova, E. S.; Krzhizhanovskaya, M. G.; Rassomakhin, M. A.; Shilovskikh, V. V.; Krivovichev, S. V. Crystal Chemistry and High-Temperature Behaviour of Ammonium Phases NH4MgCl3·6H2O and (NH4)2Fe3+Cl5·H2O from the Burned Dumps of the Chelyabinsk Coal Basin. *Minerals* **2019**, *9* (8), 486.
(55) Figgis, B.; Raston, C.; Sharma, R.; White, A. Crystal Structure of Diammonium Aquapentachloroferrate(III). *Aust. J. Chem.* **1978**, *31* (12), 2717−2720.
(56) Ackermann, M.; Brüning, D.; Lorenz, T.; Becker, P.; Bohatý, L. Thermodynamic Properties of the New Multiferroic Material $(NH_4)_2[FeCl_5(H_2O)]$. *New J. Phys.* **2013**, *15* (12), 123001.
(57) Lacková, D.; Ondrejkovičová, I.; Koman, M. A New Pathway of Preparation and Refined Structure of (NH4)2[FeCl5(H2O)]. *Acta Chim. Slovaca.* **2013**, *6* (1), 129−132.
(58) Cai, J.; Liu, J.; Gao, Z.; Navrotsky, A.; Suib, S. L. Synthesis and Anion Exchange of Tunnel Structure Akaganeite. *Chem. Mater.* **2001**, *13* (12), 4595−4602.
(59) Grundl, T.; Delwiche, J. Kinetics of Ferric Oxyhydroxide Precipitation. *J. Contam. Hydrol.* **1993**, *14* (1), 71−87.
(60) Bibi, I.; Singh, B.; Silvester, E. Akaganéite (β-FeOOH) Precipitation in Inland Acid Sulfate Soils of South-Western New South Wales (NSW. *Geochim. Cosmochim. Acta* **2011**, *75* (21), 6429−6438.
(61) Luo, Y.; Ding, J.; Shen, Y.; Tan, W.; Qiu, G.; Liu, F. Symbiosis Mechanism of Iron and Manganese Oxides in Oxic Aqueous Systems. *Chem. Geol.* **2018**, *488*, 162−170.
(62) Ahmad, A.; Van Der Wal, A.; Bhattacharya, P.; Van Genuchten, C. M. Characteristics of Fe and Mn Bearing Precipitates Generated by Fe(II) and Mn(II) Co-Oxidation with O2, MnO4 and HOCl in the Presence of Groundwater Ions. *Water Res.* **2019**, *161*, 505−516.

https://doi.org/10.1021/acsomega.5c01588
ACS Omega 2025, 10, 18085−18097